(17) Ball, R. C.; Doi, M.; Edwards, S. F.; Warner, M. *Polymer* **1981**, *22*, 1010.
(18) Adolf, D. *Macromolecules* **1988**, *21*, 249.
(19) Allen, de G. D. M. *Relaxation Methods*; McGraw Hill: New York, 1954.
(20) A junction is elastically active if three or more of its arms are independently attached to the network.
(21) Termonia, Y.; Smith, P. *Macromolecules* **1987**, *20*, 835; *Ibid.* **1988**, *21*, 2184.
(22) Termonia, Y.; Meakin, P.; Smith, P. *Macromolecules* **1985**, *18*, 2246; *Ibid.* **1986**, *19*, 154.
(23) Treloar, L. R. G. *The Physics of Rubber Elasticity*, 2nd ed.; Clarendon: Oxford, 1958.
(24) The end-to-end vectors between nodes in the initial lattice are given a length $\mathbf{r} = n^{1/2}l$, with $n = 22$ (see section 2.c.). However, the removal of nodes after cross-linking leads to larger chain vector lengths $\mathbf{r}'$, which satisfy the relation $\mathbf{r}' = n'^{1/2}l$ only in the *average* sense. Chain vectors found not to satisfy that relation had their n' value readjusted. For conversion factors $p > 0.9$, this leads to a change in the average number of statistical segments per chain vector of no more than a few percent.
(25) Ferry, J. D. *Viscoelastic Properties of Polymers*, 3rd ed.; Wiley: New York, 1980; p 374.
(26) Van Der Hoff, B. M. E.; Buckler, E. J. *J. Macromol. Sci., Chem.* **1967**, *A1*(4), 747.
(27) Valles, E. M.; Macosko, C. W. *Macromolecules* **1979**, *12*, 673.
(28) Mooney, M. *J. Appl. Phys.* **1948**, *19*, 434; Rivlin, R. S. *Philos. Trans. R. Soc. London* **1948**, *A241*, 379.
(29) Mark, J. E.; Rahalkar, R. R.; Sullivan, J. L. *J. Chem. Phys.* **1979**, *70*, 1794.
(30) Llorente, M. A.; Mark, J. E. *J. Chem. Phys.* **1979**, *71*, 682.

Chain Dynamics, Mesh Size, and Diffusive Transport in Networks of Polymerized Actin. A Quasielastic Light Scattering and Microfluorescence Study

Christoph F. Schmidt, Michael Bärmann, Gerhard Isenberg, and Erich Sackmann*

Biophysics Group, Department of Physics, Technische Universität München, D-8046 Garching b. München, FRG. *Received December 8, 1988; Revised Manuscript Received February 13, 1989*

ABSTRACT: Dynamical (chain excitations, reptational diffusion) and structural (mesh size) properties of semidilute solutions (gels) of polymerized actin and their concentration dependencies were studied by quasielastic light scattering (QELS) and microfluorescence experiments. By QELS we could measure the internal dynamics of single chains. The fact that only internal single-chain dynamics are observed by QELS is a consequence of the inverse of the scattering vector $\mathbf{q}$ (6×10^4 cm$^{-1} \leq q \leq 3 \times 10^5$ cm^{-1}) being small compared to both the average contour length of the actin filaments (≥ 30 μm), which was estimated from reptational diffusion, and the average mesh size ξ of the network. That QELS measures internal dynamics of single chains is also shown by the insensitivity of the measured dynamic structure factor to cross-linking by α-actinin. For the range of actin concentrations, 0.08 mg/mL $\leq c_a \leq$ 0.37 mg/mL, and scattering angles, $20° \leq \theta \leq 150°$, studied in this work, the dynamic structure factor $S(\mathbf{q},t)$ of the polymer chains decays like $S(\mathbf{q},t) \propto \exp(-\Gamma_q^{(0)}t)$ at short times ($\Gamma_q^{(0)}t \ll 1$). At long times ($\Gamma_q^{(0)}t \gg 1$) it follows the relation $S(\mathbf{q},t) \propto \exp(-(\Gamma_a^{(0)}t)^{2/3})$. The initial decay rate $\Gamma_q^{(0)}$ exhibits a power law of the form $\Gamma_q^{(0)} \propto q^{2.76\pm0.1}$. Actin filaments thus approximate the universal behavior predicted for a Rouse–Zimm chain by Dubois-Violette and de Gennes (*Physics* **1967**, *3*, 181). The deviation from the predicted q^3 dependence of the initial decay rate is similar to that found for synthetic polymers by several groups. Concentration-dependent deviations from Rouse–Zimm behavior, which are most prominent for $\Gamma_q^{(0)}t \gg 1$, are attributed to filament interactions. Translational diffusion coefficients of fully polymerized actin filaments were measured by fluorescence photobleaching (FRAP). We obtained a diffusion coefficient of $D_{trans} \approx 8 \times 10^{-11}$ cm^2/s for $c_a = 1$ mg/mL. D_{trans} scaled roughly like $D_{trans} \propto c_a^{-1} \propto \xi^2$ as predicted by the reptation model for flexible chains. The average mesh size of actin networks as a function of actin concentration, c_a, was determined by measuring the translational diffusion coefficient, $D(c_a,d)$, of latex spheres of various diameters, d, by both FRAP and microscopic videotracking (Perrin technique). Scaling laws were applied to relate first $D(c_a,d)$ to the ratio d/ξ and second the mesh size ξ to the actin concentration c_a. $D(c_a,d)$ scales as $D(c_a,d) = D(0,d)\exp\{-\alpha[dc_a^{\nu}]^{\delta}\}$ with $\nu \approx 1/2$, $\delta \approx 2$, and $\alpha \approx 1$ as hypothesized by de Gennes et al. for a non-cross-linked network of rodlike polymers. The Rouse–Zimm-like behavior of actin filaments, as observed by QELS, contrasts with the appearance of actin as a semiflexible polymer in microscopic end-to-end distance measurements, which have been reported in the literature. This scale-dependent difference in apparent flexibility is suggested to be a consequence of the complex structure of actin filaments as a "polymer of polymers". We hypothesize that small-scale dynamics are dominated by stretching elasticity, i.e., by Rouse–Zimm-like excitations of filament subunits, whereas large-scale dynamics are determined by the bending elasticity of the filament. The crossover length between the two regimes would have to be of the order of micrometers. We point out the usefulness of actin gels as model systems to study fundamental properties of polymers on a mesoscopic scale with coil radii in the 100-μm regime. On this scale internal motions can be easily studied by quasielastic light scattering instead of neutron scattering.

Introduction

Actin filaments are a major component of the cell cytoskeleton. They are believed to play an essential role in cell motility, intracellular transport, and in the determination of the viscoelastic properties of cells.[1] A large number of actin binding proteins (some 20–30) have been identified which regulate the polymeric structure and the viscoelasticity of the actin network as well as its coupling to the cell membrane.[1] An actin filament can be viewed either as a one-start, left-handed helix with a 5.9-nm pitch or as a two-start, right-handed helix with a 71.5-nm pitch.[2] There is experimental evidence[3] that the longitudinal bonds are stronger than the lateral bonds, thus favoring

* To whom correspondence should be addressed.

0024-9297/89/2222-3638$01.50/0

the double-helix model. The helix diameter is about 7 nm.

There exist two fundamental differences between synthetic linear polymers and polymerized actin:

(1) The former grow in a nonpolar way from both ends of the chain and cannot reanneal or grow after fragmentation. In contrast, actin filaments exhibit a fast-growing end (the so-called barbed end) and a slow-growing end (the pointed end)[4] and are in a dynamic state of continuous de- and repolymerization. A consequence of this behavior is that in the steady state of the reaction there exists a so-called critical concentration of actin monomers.[2]

(2) The polar growth of the filaments requires ATP and is thus a nonequilibrium process.[2] Once in a steady state, however, the dissociation–association process is slow compared to the thermal motions of the actin network, which can, in that respect, be considered to be an equilibrium process. Various studies of end-to-end distances by light[5] and electron microscopy[6] provide evidence that actin filaments are semiflexible chains with a persistence length of 6–25 μm.

In the present work we studied the dynamics of actin filaments in solutions of various concentrations by quasielastic light scattering (QELS).[7] Since the interpretation of QELS experiments is usually ambiguous without additional information, we performed two types of accompanying experiments. First, we measured the translational diffusion coefficient of actin filaments by fluorescence photobleaching (FRAP). Second, we determined the average mesh size of actin gels by diffusion measurements of latex spheres of various diameters in the actin gels and by making use of scaling laws relating the friction that the spheres experience to the protein concentration and the sphere radius. From these studies we could conclude that the decay of the intensity autocorrelation function of the scattered light, which is obtained in the QELS experiment, is dominated by internal dynamics of a single chain.

It will be shown that the dynamics of polymeric actin on the length scale of the light scattering experiment can be explained by the Rouse–Zimm model of polymer dynamics. Systematic deviations are discussed in terms of cooperative effects involving chain–chain interactions.

The present study is complementary to the work of Janmey et al.,[8] who concentrated on the dynamics of short actin rods, using gelsolin to fragment the filaments to lengths comparable to the inverse of the momentum transfer vector **q**.

The effect of the actin-binding protein α-actinin (a cross-linking agent) on the dynamics of actin gels was also studied.

Materials

Proteins. Actin (M_r 42000) was prepared from rabbit skeletal muscle following the method of Spudich and Watt[9] with the modification introduced by McLean-Fletcher and Pollard,[10] i.e., adding a gel column chromatography step (Sephacryl S300). After sterile filtration, monomeric actin was stored in G-buffer (see below) on ice. The protein concentration was determined by UV absorption spectroscopy at 290 nm (specific absorption, 0.65 cm^2/mg).

The quality and the purity of an actin preparation were checked by both SDS gel electrophoresis and the measurement of the hydrodynamic radius of monomeric actin by QELS. The measured diffusion coefficient of monomeric actin (concentration, 60 μM; temperature, 20 °C) of $D_{20°C} = (8.75 \pm 0.3) \times 10^{-7}$ cm^2/s is in good agreement with literature data[11-13] and corresponds to a hydrodynamic radius of $a = 2.45 \pm 0.1$ nm. The presence of actin oligomers is revealed by a decrease of the mean diffusion coefficient. Storage at 4 °C for up to 8 weeks led to a gradual decrease of $D_{20°C}$ by ~15%, which would correspond to a dimer fraction of ~7%. A fraction of the actin was labeled by 7-chloro-4-nitrobenzo-2-oxa-1,3-diazole (NBD) following the procedure of Detmers et al.[14] NBD chloride was purchased from Sigma Chemie GmbH, FRG.

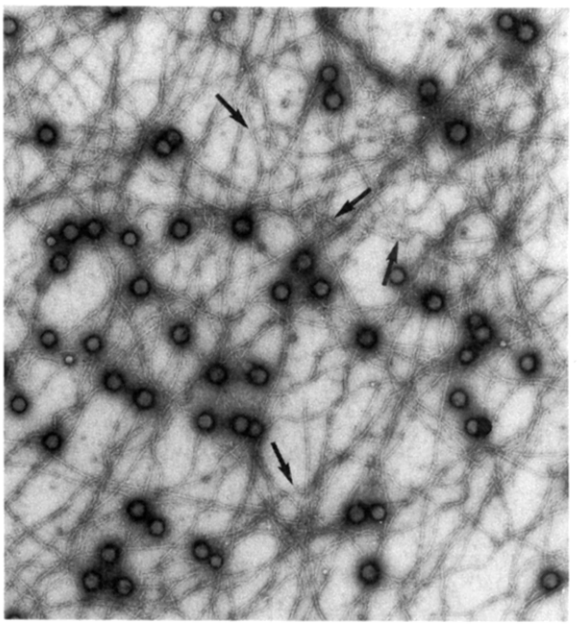

Figure 1. Typical electron micrograph of a network of fully polymerized actin. The protein concentration was 0.15 mg/mL. Negative staining with 1% uranyl acetate was used. The round spots are latex spheres of 0.1-μm diameter. Sharp bends occurring on filaments are marked by arrows.

The actin binding protein α-actinin (M_r 40000) was isolated from turkey gizzard, following the method of Craig et al.[15]

Fluorescent labeled latex spheres (Fluoresbrite TM plain microspheres, yellow green) were purchased from Polysciences Inc.

Buffers. Monomeric actin was kept in a buffer (called G-buffer in the following) which consisted of 2 mM Tris-Cl (pH 7.5), 0.2 mM $CaCl_2$, 0.5 mM DTT, and 0.2 mM adenosine 5′-triphosphate (ATP). Actin was polymerized in a 10 mM imidazole buffer (pH 7.2) (called F-buffer in the following), containing 2 mM $MgCl_2$, 1 mM EGTA, and 1 mM ATP. For some experiments F-buffer was used with the same composition except that the $MgCl_2$ concentration was reduced. In all cases the ATP was added just prior to pH adjustment to avoid hydrolysis.

A typical electron micrograph of a network of polymerized actin is shown in Figure 1. The round objects are latex spheres of 0.1-μm diameter.

Methods

Quasielastic Light Scattering. a. Experimental Setup. A sketch of the experimental setup is shown in Figure 2. The goniometer and the sample holder are specially constructed. Particular care was taken in the construction of the index matching cell and the sample holder to allow angle-dependent dynamic as well as abolute intensity measurements from a scattering angle of 150° down to 10°. As a light source an argon ion laser (Spectra Physics, 164-09) is used. The laser beam (514.5 nm, TEM_{00} mode, maximum power 150 mW) is focused in the sample by a lens, L1 (f = 150 mm). The focus diameter is ~50 μm. The primary intensity can be varied by a rotatable, silver coated, partially transparent mirror, M3. After passing through the sample the primary beam is coupled out of the cell via a rod of absorbing glass (cf. Figure 3).

For detection in the homodyne mode a photomultiplier (EMI 9865), selected for photon counting, is mounted on the arm of a goniometer table (Huber Diffractionstechnik GmbH, Rimsting, FRG). The scattering volume is limited

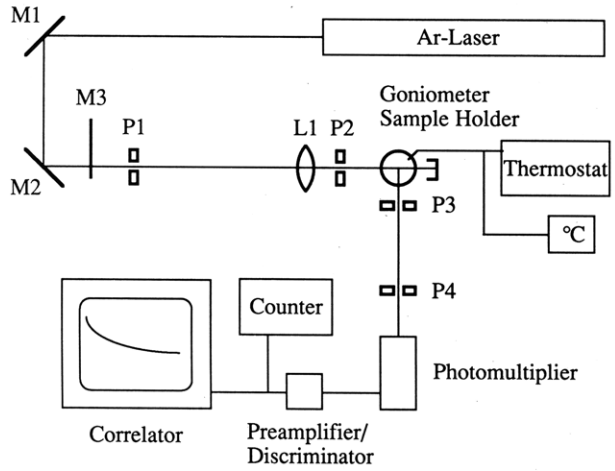

Figure 2. Sketch of the experimental setup for QELS. Explanations are given in the text.

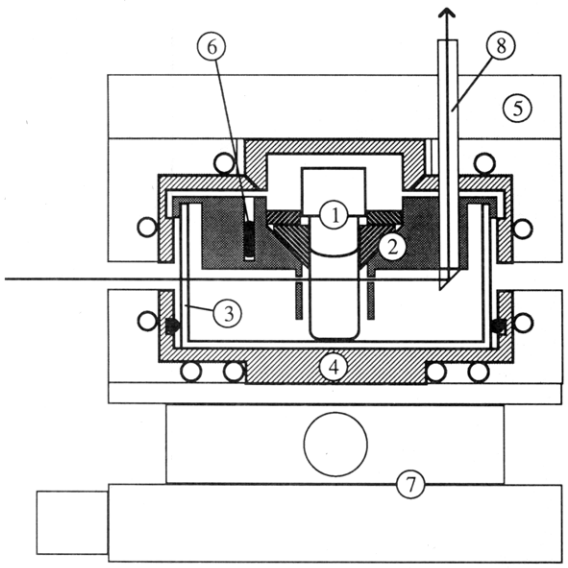

Figure 3. Measuring chamber for QELS experiments. A cylindrical glass sample cell of 12-mm inner diameter (1) is positioned in the center of an index-matching cell (3) and fixed in the aluminum lid (2) of this cell. The index-matching cell is a cylindrical, precision fabricated quartz glass container (inner diameter, 80 mm; inner height, 40 mm) with two plane-parallel quartz windows on opposite sites of the cell. It is filled with toluene as index-matching fluid. The cell is inserted in a water-thermostated copper casing (4), which is thermally isolated from the environment by a layer of polyurethane foam (5). The bath temperature is measured by a Pt-100 resistor (6). The whole chamber is mounted on an x–y stage and a tilting table (7). The primary laser beam enters through one of the plane-parallel quartz windows, passes through the sample cell, and is coupled out of the index-matching bath by a rod of absorbing glass (8).

by two pinholes, P3 and P4, of variable size, usually 0.2 mm. The optics are mounted on a massive granite bench resting on air cushions. The output of the preamplifier/discriminator (ALV-Laservertriebsgesellschaft mbH, Langen, FRG), which is integrated in the water-cooled housing of the PM tube, is fed into a digital correlator (72 channels real time, BI 2020, Brookhaven Instruments Corp.). The total scattered intensity is monitored by a pulse counter (100 MHz Counter Timer, Model 6003, Kontron Electronic, Eching, FRG). A cross section of the sample holder is shown in Figure 3. A cylindrical glass sample cell (screw cap vials, 3.7 mL, Supelchem Chromatographie Zubehör GmbH, Sulzbach, FRG) is held in the center of a cylindrical index-matching cell, made of quartz (custom fabricated by Hellma GmbH+Co, Müllheim, FRG), with two plane parallel quartz windows on opposite sides of the cell. The inner diameter of the cell is 80 mm. The index-matching cell is enclosed in a copper casing with apertures for the primary beam and the observation of the scattered light. The cell can be kept at constant temperature (±0.2 °C) by a water bath thermostat (Julabo F20, Julabo Labortechnik GmbH, Seelbach, FRG). The casing is thermally isolated from the environment by a layer of polyurethane foam. The temperature in the index-matching bath is measured by a Pt-100 resistor. Toluene is used as index-matching fluid. For adjustment the whole sample holder can be translated on an x–y stage, rotated about a vertical axis and tilted about two horizontal axes.

b. Sample Preparation and Measuring Procedure. The samples were prepared in a cleanroom under a laminar flow hood. Protein solutions and buffers were directly filtered into the detergent-cleaned (Hellmanex, Hellma GmbH+Co, Müllheim, FRG) and rinsed vials through prerinsed Millipore filters (0.2-μm pore size). The samples were stored at 4 °C before the experiments for at least 12 h to ensure full polymerization.

The scattered light was analyzed in the form of intensity autocorrelation functions with a resolution of 512 equidistant channels (see, for example, the monograph of Berne and Pecora[16] for a detailed introduction to the technique of quasielastic light scattering). Using the multiplexing capability of the correlator, the data were accumulated in eight partially overlapping blocks of 72 channels. The large number of channels was necessary since actin gels exhibit a wide range of relaxation times in the scattered light. The sampling time, Δt, was chosen in such a way that the shortest measured decay constant, Γ_{min}, corresponded to about 10 channels ($1/\Gamma_{min} \approx 10\Delta t$) and the largest decay constant, Γ_{max}, corresponded approximately to the whole width of the measured correlation function ($1/\Gamma_{max} \approx 512\Delta t$). The intensity of the primary beam was adjusted in such a way that the pulse rate was not lower than 20 KHz, but the number of overflow events of the four-bit-input counter (at small angles after prescaling) was less than 10^{-4} of the total number of counts.

The base line (usually corresponding to values of the unnormalized correlation function of the order of 10^6–10^7) was determined for each block of data both by calculating the square of the mean pulse rate (calculated base line) and by measuring the correlation function in eight delay channels (measured base line). These delay channels are delayed by $1024\Delta t$ with respect to the first channel of the respective data block. Residual dust particles or slow convective concentration fluctuations in the case of actin gels can lead to a difference between the two base-line values. Measurements at angles >40° usually showed a relative difference between the base-line values of less than 1%. Measurements with a difference larger than that were discarded. At angles <40° the relative differences were between 1% and 10%.

The intensity autocorrelation function of the scattered light, $G_2(\mathbf{q},t)$, which is in principle measured in the homodyne detection mode, can be simply expressed in terms of the electric field autocorrelation function, $G_1(\mathbf{q},t)$, if the electric field of the scattered light, $E_s(\mathbf{q},t)$, is a Gaussian stochastic variable (see ref 16, chapter 4)

$$g_2(\mathbf{q},t) = 1 + |g_1(\mathbf{q},t)|^2 \quad (1)$$

where $g_1(\mathbf{q},t) = G_1(\mathbf{q},t)/G_1(\mathbf{q},0)$ and $g_2(\mathbf{q},t) = G_2(\mathbf{q},t)/G_2(\mathbf{q},0)$ are the normalized intensity and field correlation functions, respectively.

For solutions of polymers the dynamic structure factor $S(\mathbf{q},t)$ is defined as[16]

$$S(\mathbf{q},t) = \frac{1}{n^2}\sum_{ij}^{n}\exp\{i\mathbf{q}[\mathbf{r}(t) - \mathbf{r}(0)]\} \quad (2)$$

where the summation is over the n polymer segments, located at $\mathbf{r}(t)$ at time t, belonging to one polymer molecule. In semidilute and concentrated solutions, intramolecular correlations have to be taken into account, and the summation has to run over all polymer segments of all polymer molecules in the scattering volume.

$S(\mathbf{q},t)$ is proportional to $G_1(\mathbf{q},t)$;[16] i.e., it holds that $s(\mathbf{q},t) = S(\mathbf{q},t)/S(\mathbf{q},0) = g_1(\mathbf{q},t)$. Using eq 1 and taking into account the coherence properties of the scattered light (see ref 16 for a detailed explanation), the measured data points $C(\mathbf{q},t)$ are interpreted as

$$C(\mathbf{q},t) = \langle n\rangle^2(1 + f(A)|s(\mathbf{q},t)|^2) \quad (3)$$

where $\langle n\rangle^2$ is the square of the mean pulse rate, i.e., the base line, and $f(A)$ is a so-called coherence factor (<1), which depends on the geometry of the optical setup. If $E_s(\mathbf{q},t)$ does not exhibit Gaussian statistics, $f(A)$ becomes strongly dependent on the scattering vector $\mathbf{q}$. Such an effect has been reported by Carlson and Fraser[17] for actin networks and was interpreted by them in terms of a harmonically bound particle model. In our experiments we did not observe an angle dependence of $f(A)$ at all protein concentrations studied (up to 0.3 mg/mL). Moreover, $f(A)$ measured with actin was equal to the coherence factor measured with a solution of latex spheres (0.91 μm) at small $\mathbf{q}$ under equivalent conditions. This provides strong support for our assumption that the light scattered by an actin network exhibits Gaussian statistics.

In order to test whether multiple scattering plays a role, we measured the ratio of depolarized to polarized scattered intensity for a solution with an actin concentration of 0.2 mg/mL. Since this ratio was less than 10^{-3}, multiple scattering is excluded as a source of error.

The data were normalized, according to eq 3, by division by the measured base line, subtraction of 1, and division by $f(A)$. The coherence factor $f(A)$ was determined by linear extrapolation of the first five points of the logarithm of $\{C(\mathbf{q},t)/\langle n\rangle^2 - 1\}$ to $t = 0$. Finally the square root was taken.

To obtain a distribution of decay rates from the normalized data points, $s(\mathbf{q},t)$, inverse Laplace transformation was performed on a Cyber 990E computer (Leibnitz Rechenzentrum, Technische Universität München). We used the two programs CONTIN and DISCRETE, which were kindly provided by Dr. S. W. Provencher. The programs were developed with special consideration of noise problems in light scattering data, created by the ill-conditioned nature of the Laplace inversion.[18-23] The preparation of the input files and the splicing of the eight data blocks into a continuous data set was done with a Fortran-V program. We used our modified version of a program kindly provided by Pecora and co-workers.

DISCRETE, which analyzes $s(\mathbf{q},t)$ as a sum of discrete exponentials, was used to confirm the CONTIN results. For the actin experiments the results of both programs usually were in good agreement in terms of average decay rates and number and position of peaks/components of the calculated solutions. CONTIN analyzes the measured structure factor, $s(\mathbf{q},t)$, in terms of a continuous distribution of expontentials:

$$s(\mathbf{q},t) = \int_{\Gamma_{min}}^{\Gamma_{max}} d\Gamma\, f(\Gamma)\exp(-\Gamma t) + \epsilon \quad (4)$$

The integration limits Γ_{min} and Γ_{max} are adjustable parameters and ϵ is a constant, allowing for dust or other contributions slower than $1/\Gamma_{min}$. If ϵ was not zero or near zero, the data were discarded. It is easily verified that the average decay rate, $\langle\Gamma\rangle$, obtained by division of the first moment of the distribution $f(\Gamma)$ by the zeroth moment according to

$$\langle\Gamma\rangle = \int d\Gamma\, \Gamma f(\Gamma)/\int d\Gamma\, f(\Gamma) \quad (5)$$

equals the initial decay rate, $\Gamma_q^{(0)} = d[\ln s(\mathbf{q},t)]dt|_{t=0}$, of the fitted $s(\mathbf{q},t)$. This holds, provided that as t approaches 0, the various dynamical processes contributing to $s(\mathbf{q},t)$ are essentially independent. $\Gamma_q^{(0)}$ is frequently used to characterize scattering data from polymeric systems since it can be calculated exactly from various models.[24] An average apparent diffusion coefficient $\langle D\rangle$ is calculated from $\langle\Gamma\rangle$ as $\langle D\rangle = \langle\Gamma\rangle/q^2$.

Microfluorescence Experiments. a. Experimental Setup. The experimental setup for fluorescence photobleaching (FRAP) measurements has been described in detail elsewhere.[25] It is based on an inverted Zeiss Axiomat microscope with an argon laser (Spectra Physics 2020) as light source. The laser beam passes through an electromagnetic shutter (bleach shutter) which is opened only to produce a short bleach pulse. After this shutter the beam passes through a circular pinhole of 0.4-mm diameter, which is projected into the center of the sample by a long working distance objective lens (Olympus, LWD/CD Plan 40). The diameter of the image of the aperture is 22 μm. For the observation of the fluorescence, a beam of $\sim 10^4$-fold lower intensity than the bleaching beam is produced by deviating part of the primary beam around the bleach shutter by mirrors. The fluorescence intensity was measured by photon counting, using a photomultiplier (RCA, C 31034) and a microcomputer (Apple 2). The microcomputer was also used for shutter control and data storage and evaluation.

For video tracking of fluorescent latex spheres epi-illumination with a high-pressure xenon lamp (Zeiss, XBO 75 W/2) was used. Images were taken with a SIT camera (Hamamatsu C1000) and were recorded on a video recorder (SONY, U-matic VO-5800 PS) for later evaluation.

b. Lateral Diffusion of Actin Filaments. For FRAP experiments with fully polymerized actin we used closed chambers, which consisted of an acrylic glass slab with an inserted O-ring, clamped onto a quartz microscope slide by metal clamps. The cylindrical sample volume was 15 mm in diameter and 300 μm deep. The cells were filled with freshly prepared solutions of actin (including 5% NBD-labeled actin) and polymerizing buffer (F-buffer, see above). To guarantee full polymerization, the samples were left at room temperature for at least 4 h.

For the FRAP measurements performed during the course of polymerization, a flow chamber, made of acrylic glass and tightened by an O-ring, was clamped onto a quartz slide. The rectangular sample volume had an area of 15 × 2.5 mm^2 and a depth of 1 mm. The first measurement was started immediately after filling the chamber with the freshly prepared actin/buffer solution by using a peristaltic pump connected to the outlet of the chamber. For each individual experiment a new volume of the sample was moved into the center of the field of view of the microscope.

A bleaching experiment proceeds as follows. First, the fluorescence intensity of the unbleached sample is measured for 3 s. Then the sample is bleached by a pulse of high intensity, usually of 300-ms duration. The recovery of the fluorescence intensity is recorded intermittently with exponentially increasing time steps. In order to avoid bleaching by the observation beam, the maximum exposure time of the sample is 3 s at each step. After a break of the

same length of time as the recorded recovery curve, the base-line intensity is measured for 3 s. The diffusion coefficient of the fluorophores is determined from the halftime of recovery according to the approximation given by Axelrod et al.:[26]

$$D = 0.22\frac{r^2}{t_{1/2}} \tag{6}$$

Equation 6 is valid for a bleaching and observation beam with a rectangular intensity profile. This is a good approximation in our case since the half-width of the Gaussian profile of the primary beam is about five times larger than the image plane aperture of 400 μm. The bleached and the observed volume is approximated as a cylinder of 22-μm diameter. This approximation is applicable since the angular divergence of the focused laser beam is only ~1.5°. The illuminated volume is focused on a circular aperture of 1.5-mm diameter, positioned in front of the photomultiplier. Fluorescence light from far out of the focused plane is thus excluded from detection.

Control measurements with fluorescent latex spheres show that the error introduced by the applied approximations is less than 20%. Diffusion coefficients lower than 10^{-10} cm^2/s are not exactly measurable because long time fluctuations in temperature and the mechanical setup cannot be excluded.

c. Diffusion of Latex Spheres in Actin Gels. Two methods were utilized. First, diffusion coefficients of fluorescent latex spheres were measured by FRAP as described above. Samples were prepared by mixing (unlabeled) actin with F-buffer and adding fluorescent latex spheres at a concentration of 5×10^{-3}% (w/v). Second, following the classical Perrin technique, the tracks of individual fluorescent latex spheres were recorded on videotape from the microscope and evaluated by a digital image processing system, which has been described elsewhere.[27] Samples were prepared as described above, using a latex concentration of 1×10^{-5}% (w/v). For calibration, the projection of a ruler slide with 100 marks per millimeter was recorded with the same optical setup. From each digitized video half-frame, the evaluation program first stores an 8 × 8 pixel matrix, corresponding to an area of about 4 × 4 μm^2, of intensity values around the location of the pixel with maximum intensity in the matrix stored from the preceding half-frame. The absolute location of each matrix is stored as well. This can be done in real time. The time resolution of the procedure is therefore $^1/_{50}$ s. The tracking is started and stopped manually when the particle enters and leaves the focal plane. After a series of matrices corresponding to a record length of maximally 60 s are taken, in a second step, the trace of the observed particle in the two-dimensional projection is reconstructed. The most simple procedure to define the location of the particle is to choose the pixel with the maximum intensity from each stored matrix. This procedure proved to be sufficient in the case of the fluorescent latex beads, since they produced a high contrast to the background. The trace of a single particle is finally stored as an array of x–y coordinates relative to the video frame. In a third step, the mean-square displacement of the spheres is calculated as a function of time. For that purpose a 2-fold average is performed. First, the squares of the spatial distances of all points, corresponding to a fixed distance in time on the trace of one particle (with the length of the whole evaluated trace as maximum time difference), are averaged. Second, an average over the traces of 10–30 different particles is performed, using the proper statistical weights, which increase with increasing track length. The depth of focus as well as the mean distance over which the particles could maximally be followed was about 10 μm. Thus it is assumed that there is no bias in choosing the evaluated traces from the ensemble of all possible three-dimensional diffusion paths. The diffusion coefficient, D, is therefore calculated from the mean-square displacement $\langle r^2 \rangle$ at time t by

$$D = \frac{1}{4}\frac{\langle r^2 \rangle}{t} \tag{7}$$

As a test of the method, the diffusion coefficient of 0.25-μm latex spheres was measured in F-buffer. The plot of $\langle r^2 \rangle$ versus time is close to a straight line (see Figure 10a), and the diffusion coefficient obtained from a linear regression, $D = 2.3 \times 10^{-8}$ cm^2/s, is in good agreement with the FRAP results.

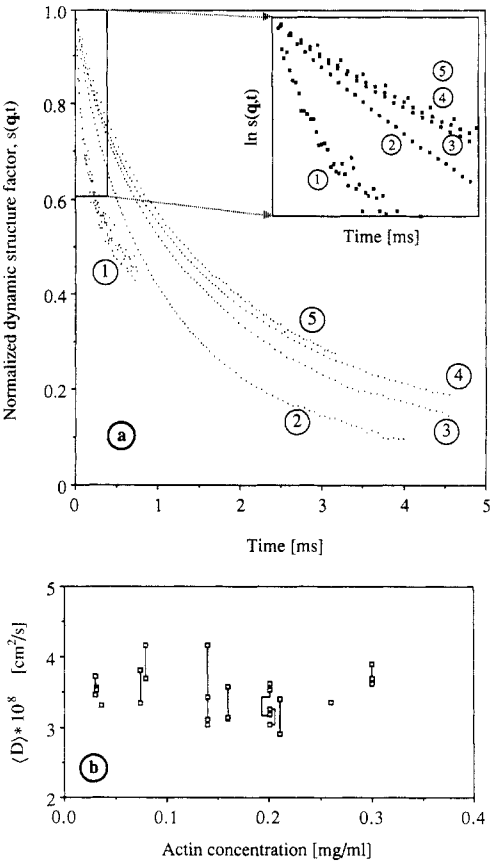

Figure 4. (a) Plot of the normalized dynamic structure factor $s(\mathbf{q},t)$ (cf. eq 2 and 3) of networks of polymerized actin at various protein concentrations (in mg/mL): (1) 0.02; (2) 0.08; (3) 0.16; (4) 0.26; (5) 0.37. Note that the time axis is normalized to 10 °C by multiplication of the real time with $\{T_x\eta(283.15K)/[283.15K\eta(T_x)]\}$, where T_x is the temperature measured during the experiment and $\eta(T_x)$ the corresponding water viscosity. The inset shows the short time behavior of the logarithm of $s(\mathbf{q},t)$ at a higher magnification. (b) Concentration dependence of the average diffusion coefficient $\langle D \rangle$ as calculated from a fit of the normalized intensity autocorrelation function of the scattered light by CONTIN. The data points were obtained from measurements of samples from various fresh protein preparations. Data points measured with the same sample are connected by a vertical bar. The plotted values are T/η scaled to 10 °C.

Quasielastic Light Scattering Experiments and Discussion

Experimental Results. Figure 4a shows the normalized dynamic structure factors $s(\mathbf{q},t)$ (cf. eq 2 and 3) of polymerized actin for protein concentrations c_a ranging from 0.02 to 0.37 mg/mL. Measurements were usually performed at 10 °C. In some cases the temperature was slightly higher or lower (9 °C < T < 12 °C). To compare

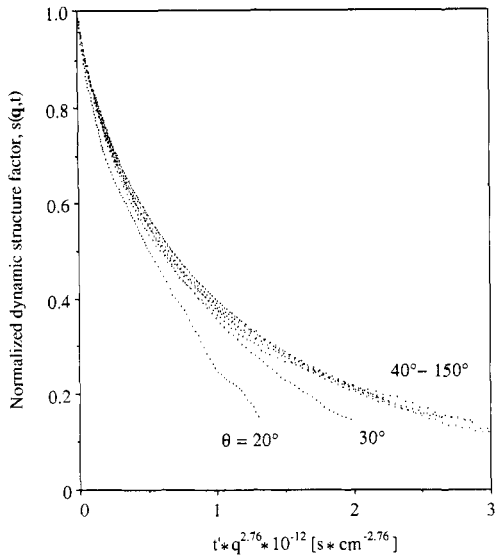

Figure 5. Angle dependence of the normalized dynamic structure factor, $s(\mathbf{q},t)$, of networks of polymerized actin at a protein concentration c_a = 0.16 mg/mL, plotted as a function of the scaled time variable: $q^{2.76}t'$. As in Figure 4a the time t' is T/η scaled to 10 °C. Measurements were performed at scattering angles θ between 20° and 150°. The curves for θ = 40°, 60°, 70°, 90°, 130°, and 150° coincide within experimental error. The curves for θ = 20° and 30° show a deviation that we attribute to the influence of cooperative chain motions.

the results obtained at a temperature T_x, the curves were normalized to 10 °C by multiplying the real time with a scaling factor $c(T)$:

$$t' = c(T)t, \qquad c(T) = \frac{T_x\eta(T = 283.15\ \text{K})}{283.15K\eta(T_x)} \tag{8}$$

where $\eta(T)$ is the viscosity of water at temperature T and T_x the sample temperature.

Figure 4a displays the following noteworthy features:

(1) The initial decay rate $\Gamma_q^{(0)}$ is approximately independent of protein concentration at concentrations higher than ~0.03 mg/mL (see Figure 4a, inset). This is more clearly visible in Figure 4b, where the average diffusion coefficient, $\langle D \rangle$, as obtained from a data fit by CONTIN (see Methods), is plotted versus the actin concentration. $\langle D \rangle$ shows no concentration dependence either.

(2) The long-time tails of the curves differ markedly for the various concentrations.

(3) The initial decay rate, $\Gamma_q^{(0)}$, increases strongly at very low concentrations (c_a < 0.03 mg/mL), which can be seen in Figure 4a. This is a consequence of the fact that at actin concentrations only slightly higher than the critical monomer concentration (see Introduction), which lies between 0.006 and 0.025 mg/mL,[28] a significant fraction of the actin is in the monomeric state, showing rapid translational diffusion. Because of the low scattering intensities at low actin concentrations, data for c_a < 0.03 mg/mL were too noisy to be evaluated by CONTIN.

It is well-known that the internal dynamics of a polymer chain can be described by a Langevin equation (see ref 29, chapter 4.1, and ref 30 and 31). This equation is usually linearized and solved by decomposing the motion of the polymer into independent modes, characterized by wavevectors **k**. The decay rate of the overdamped modes is proportional to k^p, where the expontent p depends both on the type of the elastic restoring force and the mechanism of friction. As a consequence of this power law, the normalized dynamic structure factors of the polymer for various scattering vectors **q** should coincide if they are plotted versus a reduced time $t'q^n$ with another scaling

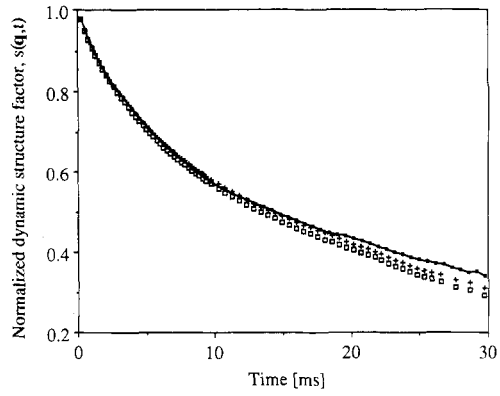

Figure 6. Effect of α-actinin on the normalized dynamic structure factor $s(\mathbf{q},t)$ of polymeric actin networks at a protein concentration c_a = 0.25 mg/mL in F-buffer. Actin to α-actinin molar ratios were (+) 60:1 and (○) 15:1. The drawn curve was obtained from a control sample which contained no α-actinin. The scattering angle was 30°, the temperature 10 °C.

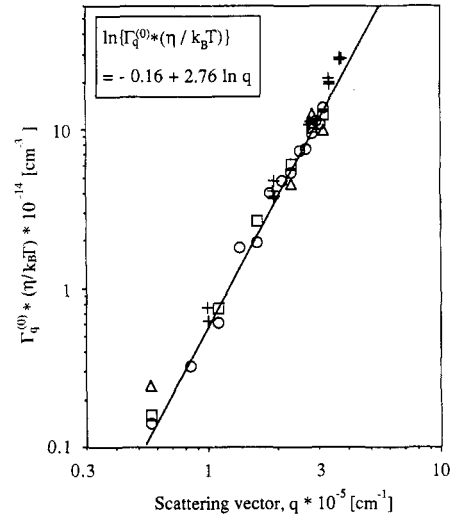

Figure 7. Double-logarithmic plot of the reduced initial decay rate, $\Gamma_q^{(0)}(\eta/T)$, of the normalized structure factor, $s(\mathbf{q},t)$, versus scattering vector q for three actin concentrations: (△) 0.26 mg/mL; (○) 0.16 mg/mL; (□) 0.08mg/mL. For comparison we plotted data from polystyrene (M_r 24 × 10^6) in good solvent (benzene) measured by QELS by Nemoto and co-workers.[33] Data points are denoted by crosses (+) and were taken from Figure 7 of ref 33. In the inset slope and intercept of the linear regression line (drawn line) of the data measured with the 0.16 mg/mL actin sample are given.

exponent n (see ref 29, chapter 4). This is, of course, only valid if the light scattering is determined by *one* physical mechanism. As can be seen from Figure 5, the curves for angles ≥40° coincide astonishingly well for a nonintegral exponent n = 2.76.

Figure 6 shows the effect of various concentrations of a cross-linking protein, α-actinin, on the dynamic structure factor of actin solutions at a low scattering angle, θ = 30°. Within experimental errors the curves coincide with that of the pure actin.

Rouse–Zimm Behavior of Actin Gels. In Figure 7 the reduced initial decay rates $\Gamma_q^{(0)}\eta/T$ are plotted against the scattering vector **q** on logarithmic scales for various samples with different actin concentrations. Data points in the figure are averages of the values obtained by CONTIN and DISCRETE. To a good approximation they lie on a straight line, revealing that $\Gamma_q^{(0)}$ follows a power law: $\Gamma_q^{(0)} \propto q^n$. By linear regression we find

$$\Gamma_q^{(0)}\frac{\eta}{T} = Bq^{2.76\pm0.1} \tag{9}$$

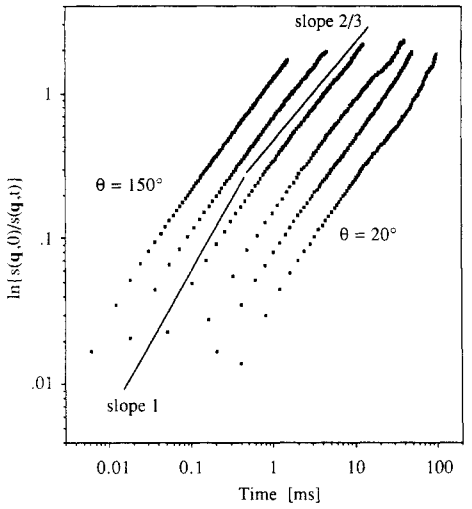

Figure 8. Asymptotic time dependence of the normalized dynamic structure factor $s(\mathbf{q},t)$ for short ($\Gamma_q^{(0)}t \ll 1$) and long ($\Gamma_q^{(0)}t \gg 1$) times. The logarithm of ln $s(\mathbf{q},t)$ is plotted versus the logarithm of time. The time axis is T/η scaled to 10 °C (cf. Figure 4a). The actin concentration was 0.16 mg/mL. The scattering angles were, from left to right, 150°, 90°, 60°, 40°, 30°, and 20°. The drawn lines have a slope of $^2/_3$ and of 1, respectively.

with B = 1.22 (cf. Figure 7).

A similar power law, also found by QELS, has been reported for high molecular weight polystyrenes in a good solvent.[32,33] Various experiments with polystyrene in good solvent, resulting in power laws also with an exponent around 2.8 for supposedly the same physical reasons, have been summarized by Delsanti.[34]

It can be seen from Figure 7 that not only the exponent of the scattering vector $\mathbf{q}$ but also the constant B in eq 9 agree very well for the synthetic and the biological polymer.

The above findings strongly suggest that the chain dynamics of actin filaments can be described in terms of the Rouse–Zimm model of polymer dynamics.[35,36] This implies that the decay of the thermal excitations of the filaments is determined by the entropy elasticity and the hydrodynamic interactions between filament segments.

As a further test of the validity of the Rouse–Zimm model, we examined the asymptotic behavior of the curves shown in Figure 4a at short ($\Gamma_q^{(0)}t \ll 1$) and long times ($\Gamma_q^{(0)}t \gg 1$). As can be seen in Figure 8, for short times $s(\mathbf{q},t)$ is a exponential function of time: $s(\mathbf{q},t) \propto \exp(-\Gamma t)$, whereas for long times $s(\mathbf{q},t)$ follows the relation $s(\mathbf{q},t) \propto \exp\{-(\Gamma t)^{2/3}\}$. Such a behavior is in agreement with the calculations of Dubois-Violette and de Gennes[30] which predict for $\Gamma_q^{(0)} \ll 1$ (cf. ref 29, chapter 4.4)

$$s(\mathbf{q},t) \propto \exp(-\Gamma_q t), \qquad \Gamma_q = \frac{k_B T}{6\pi\eta} q^3 \tag{10}$$

and for $\Gamma_q^{(0)}t \gg 1$ (cf. ref 29, chapter 4, Appendix 4III)

$$s(\mathbf{q},t) = \exp\{-1.35(\Gamma_q t)^{2/3}\} \tag{11}$$

where Γ_q is the same as in eq 10.

Deviations from the Rouse–Zimm Behavior. There are small but detectable deviations from the Rouse–Zimm behavior.

(1) As noted above (cf. Figures 5 and 7), the decay rate $\Gamma_q^{(0)}$ is not strictly dependent on the third power of $\mathbf{q}$, but rather the exponent is clearly smaller, namely, 2.76 ± 0.1 (see Figure 7). Such a deviation, however, is also typical for synthetic, flexible polymers. Several explanations have been proposed. Benmouna and Akcasu[37] have argued that the discrepancy is due to the fact that the number of independent segments in each chain is finite. Since the expected correlation length for motions of the actin network, i.e., the average mesh size ξ, is of the same order of magnitude as the wavelength of light, we cannot discard this explanation. On the other hand, the q^3-dependence, which can in the general case be inferred from scaling arguments,[38] holds only if the static and the dynamic characteristic lengths obey the same power law with respect to the number of segments, N. Adam and Delsanti[32] have shown that an exponent smaller than 3 can be obtained if this postulate is given up. In the latter case, the resulting exponent does not depend on the degree of polymerization. In view of the fact that the synthetic and the biological polymers exhibit the same exponent despite their widely different coil radii, we conclude that the hypothesis of Adam and Delsanti is the more appropriate explanation.

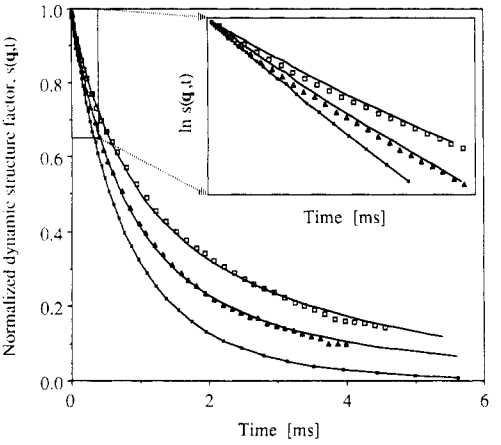

Figure 9. Comparison of two measured dynamic structure factors (□, △) with the curve calculated for a Rouse–Zimm chain under Θ-conditions by Dubois-Violette and de Gennes[30] (lower curve, ■). (□) Measured curve for an actin concentrations of 0.16 mg/mL; (△) the same for 0.08 mg/mL. The scattering angle was 90°. The time for the measured curves is T/η scaled to 10°C (cf. Figure 4a). The Rouse–Zimm curve was calculated numerically according to eq 12. The measured curves were fitted by a superposition of the Rouse–Zimm dynamic structure factor and a single exponential (cf. eq 13), and the resulting curves are shown as drawn lines. In the inset the short-time behavior of the curves is shown on a logarithmic scale.

(2) Another deviation from Rouse–Zimm behavior is illustrated in Figure 9. Measured dynamic structure factors are compared to the curve calculated from the following equations, which are valid for a Rouse–Zimm chain under θ-conditions and were first derived by Dubois-Violette and de Gennes:[30,31]

$$s_{RZ}(\mathbf{q},t) = \int_0^\infty du \exp[-u - (\Gamma_q t)^{2/3} h(u(\Gamma_q t)^{-2/3})] \tag{12}$$

with

$$h(y) = \frac{2}{\pi}\int_0^\infty dx \frac{\cos(xy)}{x^2}(1 - \exp(-x^{3/2}/2^{1/2}))$$

and

$$\Gamma_q = \frac{k_B T}{6\pi\eta} q^3$$

where η is the solvent viscosity. The integration of eq 12 was performed numerically, and the calculated curve for a scattering angle of 90° is plotted in Figure 9. Obviously, the short-time behavior of $s(\mathbf{q},t)$ is rather well described by the model, whereas at long times large deviations are observed, which are most pronounced at high protein concentrations.

It appears that the long-time tail of $s(\mathbf{q},t)$ is influenced by an additional slow dynamical process. In order to determine the concentration and q dependence of this slow process, we fitted the experimental data by a superposition of the above Rouse–Zimm structure factor and a single exponential function according to

$$s(\mathbf{q},t) = (1 - a)s_{RZ}(\mathbf{q},t) + a \exp(-\Gamma_s t) \quad (13)$$

Twelve $s(\mathbf{q},t)$ versus t curves measured for different scattering vectors $\mathbf{q}$ and 12 such curves measured for different actin concentrations were fitted by varying the amplitude, a, and the decay rate, Γ_S, of the exponential in eq 13. As initial decay rates Γ_q (see eq 12) of the Rouse–Zimm contributions $s_{RZ}(\mathbf{q},t)$, the values $\Gamma_q^{(0)}$ from the CONTIN fit to the experimental curves were used. As can be seen from the examples shown in Figure 9, the experimental curves are fitted reasonably well, although systematic deviations are still visible. The prominent results of the above analysis are (data not shown) the following:

(1) The decay rate of the slow component scales with nearly the same power of the scattering vector $\mathbf{q}$, namely, $\Gamma_S \propto q^{2.6}$, as the intial decay rate $\Gamma_q^{(0)}$ of the measured dynamic structure factor.

(2) The amplitude of the slow component does not depend on the wavevector $\mathbf{q}$.

(3) The amplitude, a, increases roughly linearly with the protein concentration from $a \approx 0.2$ at $c_a = 0.03$ mg/mL to $a \approx 0.5$ at $c_a = 0.37$ mg/mL. The decay rate Γ_S does not depend on the actin concentration.

What is the origin of the slow component? The fact that the amplitude increases with increasing protein concentration suggests that the long-time tail of $s(\mathbf{q},t)$ is governed by the coupling of the long-wavelength modes of the single-chain dynamics to cooperative motions of the ensemble of filaments. This interpretation is further supported by the finding that the slowly decaying part of $s(\mathbf{q},t)$ exhibits approximately the same q dependence as the fast-decaying (single-chain) excitations. Further experiments are necessary to clarify this point.

Diffusion of Latex Spheres in Fully Polymerized Actin Networks and Measurement of Mesh Sizes by the Application of Scaling Laws

The hindered diffusion of fluorescent labeled latex spheres of three different diameters $d = 0.07$, 0.1, and 0.25 μm in actin gels of various concentrations was measured by FRAP. In addition, the diffusion of the 0.25-μm spheres was measured by the classical Perrin technique. Typical measurements by the latter method of the mean-square displacement $\langle r^2 \rangle$ of individual spheres versus time are shown in Figure 10a. As was mentioned before, the plots are very close to straight lines, which means that the data follow very well the Einstein relation, $\langle r^2 \rangle / t$ = constant.

As shown in Figure 10b, the diffusion coefficient $D(c_a,d)$ decreases exponentially with increasing protein concentration c_a. By plotting ln {ln $[D(0,d)/D(c_a,d)]$} versus c_a for a sphere diameter $d = 0.25$ μm (see Figure 10c), we find the power law

$$D(c_a,d) = D(0,d) \exp(-\alpha(d) c_a^{1.02\pm0.1}) \quad (14)$$

where $\alpha(d)$ is concentration independent. For $D(0,d)$ we used the value obtained by extrapolation of $D(c_a,d)$ to $c_a = 0$, rather than the values measured in pure buffer. The former values were found to be ~20% smaller than the latter. We attribute this difference to adsorption of actin on the spheres, leading to a larger diameter.

Another exponential power law is observed for the dependence of the diffusion coefficient $D(c_a,d)$ on the particle diameter d as follows from Figure 10d. A linear regression yields

$$D(c_a,d) = D(0,d) \exp(-\alpha'(c_a) d^{2.14(+1)(-0.3)}) \quad (15)$$

where $\alpha'(c_a)$ is independent of the sphere diameter. Power laws in agreement with the observed dependencies have been predicted by de Gennes and co-workers for non-cross-linked networks of elongated (rodlike) polymers (polyelectrolytes) on the basis of scaling arguments.[39,40]

First, the average distance between two points of entanglement between different molecules and thus the average mesh size ξ in semidilute solutions are predicted to scale as[39]

$$\xi \propto c^{-1/2} \quad \text{for rodlike (such as polyelectrolytic) macromolecules} \quad (16a)$$

and

$$\xi \propto c^{-3/4} \quad \text{for flexible (neutral) macromolecules} \quad (16b)$$

where c is the polymer concentration of the solution.

Second, de Gennes et al.[40] conjectured that the friction coefficient $f = k_B T/D$, experienced by a particle of diameter d in a network of average mesh size ξ, is a univeral function of d/ξ. From the assumption that the motion of the particle through the network is an activated process

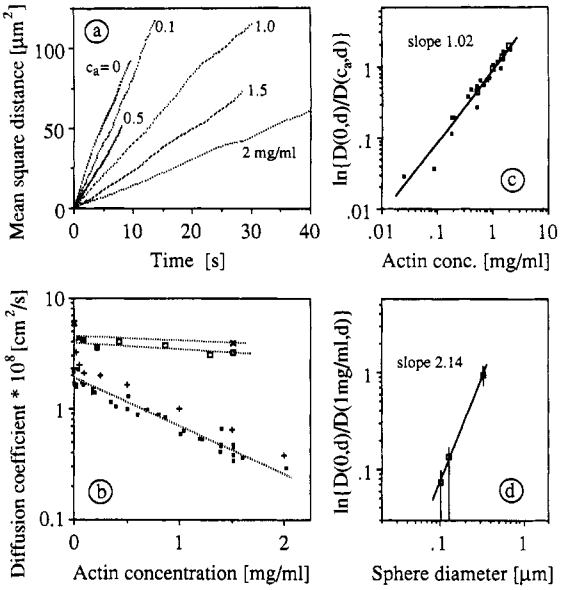

Figure 10. Diffusion of latex spheres in actin networks at a temperature of (24 ± 2) °C. (a) Plot of the mean-square displacement of latex spheres of 0.25-μm diameter as a function of time, measured by microscopic video tracking of single spheres. Each curve is an average over the tracks of 10–30 single spheres, followed for maximally 60 s. Actin concentrations in mg/mL are indicated at the curves. (b) Decrease of the diffusion coefficients, $D(c_a,d)$, of latex spheres of diameters 0.25 (■ and +), 0.1 (□), and 0.07 μm (×) in actin networks with increasing actin concentration. Diffusion coefficients were measured by FRAP at a temperature of 25 °C. The data for the 0.25-μm beads were obtained by several independent series of FRAP experiments (■) and by video tracking of single spheres (+). (c) Plot of ln {ln $[D(0,d)/D(c_a,d)]$} versus the logarithm of the actin concentration, c_a. The data points are those measured by video tracking [cf. (a)] and by FRAP [cf. (b)] with the 0.25-μm spheres. The exponent of the power law relating D to c_a was obtained by linear regression (drawn line). $D(0,d)$ was determined, for the video tracking and for the FRAP experiments separately, by extrapolation of the respective data to $c_a = 0$. (d) Variation of the diffusion coefficient, $D(c_a,d)$, with the particle diameter, d. After interpolating the data in (b), ln {ln $[D(0,d)/D(c_a,d)]$} for a fixed protein concentration c_a of 1 mg/mL is plotted versus the logarithm of the particle diameter. The power law exponent is again determined by linear regression (drawn line).

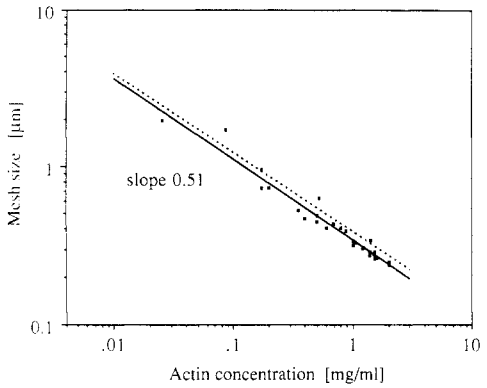

Figure 11. Double-logarithmic plot of the mesh size of actin networks, as obtained by latex sphere (0.25-μm diameter) diffusion measurements (see Figure 10), versus protein concentration. The mesh size was calculated according to scaling laws as described in the text (eq 16a and 17). The drawn line is the linear regression of the data points; the dashed line shows the mesh size calculated by assuming a cubic lattice of infinitely long rigid rods with the same diameter, d_a, as actin filaments (d_a = 7 nm).

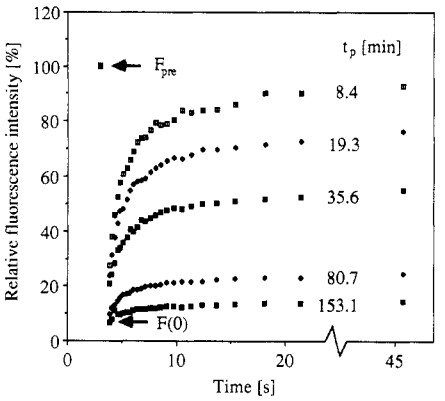

Figure 12. Fluorescence recovery curves of polymerizing actin, containing 5% NBD-labeled actin, with a total protein concentration of 1 mg/mL in F-buffer (1.5 mM Mg^{2+}), recorded at different times t_p after the start of the polymerization. F_{pre} and $F(0)$, which are indicated by arrows, are the fluorescence intensities prior to and immediately after bleaching, respectively. The temperature was 20 °C.

it follows for the diffusion coefficient $D = D_0 \exp(-\Delta G/k_BT)$, where D_0 is the diffusion coefficient of the spheres in pure solvent. Assuming furthermore that the activation energy ΔG is determined by the elastic free energy associated with the expansion of a mesh, formed by Gaussian chains, from ξ to d, which is $\Delta G \simeq k_BT(d/\xi)^\delta$, de Gennes et al.[40] arrived at the relation

$$D = D_0 \exp(-\beta(d/\xi)^\delta) \quad (17)$$

For cross-linked networks the exponent δ is 2.5, for non-cross-linked networks δ equals 2.0. The dimensionless coefficient β is expected to be of the order of one. By combining eq 16a and 17, we finally obtain

$$D(c_a,d) = D(0,d) \exp(-\beta' d^2 c_a) \quad (18)$$

The constant β' has the dimension length/mass.

This equation fits the experimental data in Figure 10b,c. The average mesh size ξ was therefore determined from these data by eq 18. The results are shown in Figure 11. In this figure we also plotted the concentration dependence of the lattice constant l_c of a cubic lattice, formed by infinitely long rods of the diameter d_a = 7 nm (equal to that of actin filaments), and of a mass density ρ typical for proteins, ρ = 1300 mg/cm^3, according to

$$l_c = \left(\frac{\rho 3\pi d_a^2}{4c_a}\right)^{1/2} \propto c^{-1/2} \quad (19)$$

where c_a is the protein concentration in milligrams per milliliter. Comparing this lattice constant to the average mesh size, ξ, determined above, it is found that $l_c = 1.13\xi$. This result supports the assumption that the constant β in eq 17 is of the order of one.

Similar measurements of particle diffusion in polymer solutions have been performed by various groups. Gorti and Ware[41] also used the FRAP technique and found for high molecular weight polyelectrolytes under low salt conditions a scaling law, $D/D_0 \propto \exp(-\alpha c)$, in agreement with the present finding. From several experiments with flexible polymers, scaling exponents between 0.5 and 1 for the concentration dependence have been reported.[41-45] In all these cases, however, it seems to have been difficult to correct for the mobility of the polymer itself. This is no problem in the case of the actin gels since the filaments are virtually immobile (see below). There exist several theoretical approaches to the problem,[46-48] which are different from the aforementioned considerations of de Gennes and co-workers. However, since our data are well fitted only by the latter theory, we do not discuss the other approaches here.

Reptational Diffusion of Actin Filaments

The translational diffusion coefficient of trace-labeled actin filaments in semidilute solutions was measured by FRAP. Figure 12 shows fluorescence recovery curves from an actin solution (c_a = 1 mg/mL) at various times t_p after the start of the polymerization. For polymerization F-buffer with 1.5 mM Mg^{2+} was used. The fluorescence intensities F_{pre} and $F(0)$ were measured prior to and immediately after bleaching, respectively. From the beginning of the polymerization the curves reflect two easily separated recovery processes. One is fast with a halftime of about 1 s; the other is too slow to be followed completely during the experiment. Such a situation is to be expected from the well-established finding that nucleation is the rate-limiting step of actin polymerization and that the filament growth is very fast.[2,49] Thus virtually only monomers and very long filaments will be present. After sufficiently long time (>4 h) of polymerization a steady state is reached, where the residual monomer concentration is equal to the critical monomer concentration c_{crit}.

From the relative amplitude of the fast recovery for a sample with a concentration c_a of 0.02 mg/mL (polymerized with 2 mM Mg^{2+}, data not shown), we estimated the critical concentration as c_{crit} = 0.008 mg/mL.

In an additional set of experiments the reptational diffusion coefficient of actin filaments was measured in samples in the steady state. The concentrations of these samples were above 0.5 mg/mL, and the actin was polymerized with 2 mM Mg^{2+}. The contribution of monomer diffusion (<1%) was neglected. The relative recovery after a recording time of ~20 min was less than 25% in all cases. In order to estimate diffusion coefficients, we assumed that for $t = \infty$ the recovery would reach 100% and approximated the curves of fluorescence intensity $F(t)$ versus time t by the following simple exponential:

$$F(t) = F(\infty)\left(1 - \frac{F(\infty) - F(0)}{F(\infty)} \exp(-t/\tau)\right) \quad (20)$$

where $\tau = 5.76D/r^2$, r is the radius of the bleached cylinder, $F(\infty)$ is the intensity after completed recovery (assumed to be equal to the prebleach intensity, F_{pre}), and $F(0)$ is the intensity directly after bleaching.

This is the first-order approximation to the solution of the differential equation describing the diffusion into an

Table I
Translational Diffusion Coefficients, D_{trans}, of Actin Filaments, Measured by FRAP, in Actin Gels of Various Protein Concentrations, c_a[a]

sample	rel recovery after 1170 s, %	c_a, mg/mL	D_{trans}, cm^2/s	L_{coil}, μm	L_{rod}, μm
1	25.1	0.5	3.75×10^{-11}	38	637
2	19.7	1.0	3.59×10^{-11}	27	665
3	13.1	1.5	2.33×10^{-11}	28	1025

[a] The last two columns give calculated values of the contour length of actin filaments: L_{coil} according to the flexible chain reptation model, eq 21, and L_{rod} according to the rigid-rod reptation model, eq 22.

infinitely long cylinder, valid for long times (see ref 50, paragraph 20A). It satisfies the boundary conditions that the fluorophore concentration is constant at all times at the cylinder surface and constant at a different level within the cylinder at $t = 0$, which corresponds to a rectangular bleaching profile. The characteristic time τ is obtained from the experimental recovery curves by a linear regression of the final part of a plot of $\ln \{[F(t)/F_{pre}] - 1\}$, where the data points usually are distributed very close along a straight line. Obviously it is a crude approximation to consider only the slowest exponential contribution, although the relative recovery lies only between 10% and 25%. However, in view of the uncertainty of the base line and possible systematic errors, the measurements are not expected to yield more than an estimate of an upper limit of the diffusion coefficient. Especially convective flow or mechanical instabilities can lead to systematic errors. The calculated values for the diffusion coefficient are summarized in Table I.

It is intriguing to compare the above results with the predictions of the reptation model of diffusion.[51] For flexible chains, the diffusion coefficient for times that are long compared to the longest relaxation time of the orientational correlation function is proportional to the square of the ratio of the mesh size ξ to the number N of independent chain segments (see ref 29, chapter 6):

$$D_{trans} = \frac{k_B T \xi^2}{9\pi\eta N^2 d_a^3} \quad (21)$$

where η is the solvent viscosity. The diameter of a segment, d_a, is assumed to be equal to the actin filament diameter: $d_a = 7$ nm. For the mesh size, ξ, the values measured with latex particle diffusion, as described in the preceding paragraph, were used. According to eq 16a and 21, D_{trans} should scale with the protein concentration, through ξ, as $D_{trans} \propto c^{-1}$. As seen from Table I, D_{trans} decreases by a factor of 1.6 if c_a is increased by a factor of 3, which is at least in rough agreement with the theory. The contour lengths, $L_{coil} = Nd_a$, calculated from eq 21 are given in Table I, column 5.

As another limiting case, we can treat the filaments as rigid rods. According to Doi and Edwards (see ref 29, chapter 9), the reptational diffusion coefficient in this case is

$$D_{trans} = \frac{k_B T \ln (L_{rod}/d_a)}{6\pi\eta L_{rod}} \quad (22)$$

where d_a is the diameter and L_{rod} the length of the rod. In this model D_{trans} does not depend on the protein concentration. Again assuming $d_a = 7$ nm, we arrive at the contour lengths given in the sixth column of Table I. The values calculated from the two models differ by more than an order of magnitude. The mean-square displacement of the center of mass of a chain with a given contour length per unit time is expected to be larger for the rigid rod than for the coiled chain since D_{trans} scales as $D_{trans} \propto 1/N^2$ for a coil and as $D_{trans} \propto \ln (N)/N$ for a rod. The real lengths of the semiflexible actin filaments will thus lie somewhere between the two extreme values of 30 and 1000 μm. The measured diffusion coefficients are in approximate agreement with the results of other groups.[13,52,53] Filament lengths of more than 10 μm are not in contradiction to the currently accepted kinetic models of actin polymerization.[54]

A tacit assumption in all the above calculations is that there is no interaction between filaments excpet for steric hindrance. It has been argued,[55-57] however, that low apparent diffusion coefficients could be a consequence of small residual concentrations of actin cross-linking proteins (e.g., α-actinin) or of a weak attractive interaction between the filaments themselves. From SDS gel electrophoresis, contaminations can be estimated to be less than 2%. Together with relatively large filament lengths, however, smaller contaminations could still have a marked effect on the translational diffusion. The same holds true for weak direct filament interactions. Cortese and Frieden recently reported evidence[58] for the existence of attractive forces from the observation of shear induced bundling of filaments.

It should be noted that these considerations are not relevant for the interpretation of the QELS data, since for QELS no assumption was made regarding the mechanism by which translational and rotational diffusion were suppressed.

Janmey et al.[8] suggested that during the process of photobleaching, photochemical reactions might cross-link the filaments. We studied the decay of mechanically induced optical birefringence in a polarization microscope[59] and found that the relaxation times of oriented, birefringent structures in the actin gels were extremely long and consistent with the very low filament mobilities observed by FRAP.

Concluding Discussion

The present study shows that on the length scale of the QELS experiments, that is 200 nm $\leq 2\pi/q \leq$ 2000 nm, the dynamics of thermal exitations of actin filaments in semidilute solutions can be well described in terms of the universal Rouse–Zimm model. Small but notable deviations from the behavior predicted by the model were found.

(1) The initial decay rate of the dynamic structure factor $s(\mathbf{q},t)$ as well as the whole curves scale with the nonintegral power 2.76 ± 0.1 of the scattering vector instead of the expected power of 3. This same deviation from Rouse–Zimm behavior, however, has been reported for synthetic polymers in good solvent.[32,37]

(2) A concentration-dependent slowing down of the long time decay of $s(\mathbf{q},t)$ was observed. It can be accounted for by an additional exponential with a decay rate Γ_s, the relative amplitude of which increases with the protein concentration. Γ_S is an order of magnitude smaller than the initial decay rate, $\Gamma_q^{(0)}$, and varies with about the same power of $\mathbf{q}$ as the latter. Moreover, Γ_S is roughly concentration independent. The slow decay is tentatively explained as an effect of the coupling of the long-wavelength excitations of single chains to cooperative concentration fluctuations.

Our interpretation of the QELS data relies on the results of additional microfluorescence experiments, the pertinent results of which are the following:

(1) Translational diffusion of actin filaments in semidilute solutions ($D_{trans} \leq 1 \times 10^{-10}$ cm^2/s) cannot account for the range of decay rates observed by QELS, which

corresponds to apparent diffusion coefficients larger than 2×10^{-9} cm^2/s.

(2) The average mesh size of the actin gels is larger than ~500 nm for all protein concentrations studied by QELS ($c_a \leq 0.3$ mg/mL). Therefore QELS is mainly determined by single chain motion. Only at scattering angles smaller than 40° cooperative effects (mesh size fluctuations) are expected to become visible, which is indeed seen in the data shown in Figure 5.

Our conclusion, based on the results of the microfluorescence experiments, that translational diffusion does not produce a major contribution to the dynamic structure factor of polymerized actin, is in contrast to the interpretation of QELS experiments performed with actin gels by Fujime and co-workers.[60] These authors postulate translational diffusion as the dominant mechanism and attribute deviations from q^3 behavior of the decay rate of the dynamic structure factor to flexural chain excitations. The filament lengths obtained from their QELS experiments, of the order of 1 μm, appeared to be in reasonable agreement with the average lengths determined from electron microscopy. However, they do not agree with the FRAP experiments of the present work and of other laboratories.[13,52,53] According to our experience with electron microscopy, this technique tends to underestimate actin filament lengths, owing to disruption of the filaments by the shear flow arising during preparation.

Janmey et al.[8] studied actin filaments fragmented by gelsolin, using QELS and electron microscopy, and interpreted the QELS results in terms of translational and rotational diffusion of rigid rods. For high gelsolin concentrations they found good agreement between the filament lengths determined by QELS and those determined from the electron micrographs. However, they leave open the questions concerning the dynamical mechanisms responsible for the QELS spectra in the case of low and zero gelsolin concentrations.

The high degree of flexibility of polymerized actin, revealed by the present QELS study, is surprising in view of the results of the elegant microscopic measurements of end-to-end-distances by three Japanese groups,[5,6,61] who find persistence lengths between 6 and 25 μm for actin filaments. This ambivalent behavior might be a consequence of the complex construction of the filaments as a polymer of macromolecular subunits. If we describe the thermal excitations of the chain in terms of a Langevin equation, the restoring force is determined both by bending and entropy (Rouse) elasticity, where the latter if formally equivalent to a stretching elasticity.[62] Since the mean-square amplitudes are proportional to q^{-4} for the bending and to q^{-2} for the stretching (Rouse) modes,[62] the former dominate the long-wavelength and the latter the short-wavelength modes. The end-to-end-distance is determined by the long-wavelength modes and is thus governed mainly by the flexural rigidity. Obviously, there is a crossover wavevector q_c above which the Rouse or stretching modes dominate. Provided that q_c is of the order of the wavevector of the scattered light, the QELS spectra would be determined by the Rouse or stretching modes.

A Rouse-like behavior could also be caused by transient local defects on the double-stranded filaments. Mobile local defects—or solitons—have been reported recently for DNA by Grimm et al.,[63] who performed quaiselastic neutron scattering studies. Evidence that such defects occur in actin filaments has recently been provided by Aebi et al.[3] These authors found indications of local unwinding of actin filaments from high-resolution electron microscopy. The existence of such a phenomenon implies that the interaction between adjacent monomers on different strands in much smaller than the monomer–monomer coupling along the strands. Further evidence, either for a high degree of local flexibility or for the existence of local hingelike regions, is provided by the fact that actin filaments frequently exhibit sharp bends besides the usual gradual curvature on electron micrographs (see Figure 1).

It should be mentioned that according to Allegra and co-workers[64] a $q^{8/3}$ scaling of the dynamic structure factor of polymers could also be explained in terms of a Rouse model including intrinsic chain stiffness.

The essentially universal Rouse–Zimm behavior of the actin filaments makes them an interesting model system from a purely physical point of view. Owing to their large end-to-end-distances of probably some 100 μm, they allow the study of fundamental physical properties of polymers on an almost macroscopic scale, where, for instance, light scattering instead of neutron scattering techniques can be applied. A further advantage, which is important for light scattering experiments, is that on the scale of the wavelength of light, solutions of polymerized actin can be treated as monodisperse systems. This is a consequence of the polymerization mechanism which leads to virtually only two coexisting populations, a small critical concentration of actin monomers on the one hand and very long filaments on the other hand. Furthermore, there are many ways to influence the state of networks of polymerized actin, for instance by actin-binding proteins, and thus to change physical parameters of the system.

The dynamics of thermal chain excitations of biological and synthetic macromolecules with largely different structures appear to follow the same power law over several orders of magnitude in length scale. It may be hoped that by regarding the characteristic differences between those systems, it will be possible in the future to find simple universal principles from the confusing variety of possible mechanisms to describe this behavior.

Acknowledgment. This work was supported by the Sonderforschungsbereich 1327 of the Deutsche Forschungsgemeinschaft, the Fonds der chemischen Industrie, and the Freunde der Technischen Universität München. We thank Prof. Dr. R. Pecora (Stanford, CA) for stimulating and helpful discussions and for sending us computer programs developed by his co-workers. We are indebted to Dr. S. W. Provencher (Göttingen, FRG) for providing the programs CONTIN and DISCRETE. Furthermore we are grateful to Dr. M. Schmidt (Mainz, FRG) and Dr. J. G. H. Joosten (Geleen, Netherlands) for enlightening discussions about the QELS technique and to Dr. M. Schleicher (Martinsried, FRG) and Dr. A. Wegner (Bochum, FRG) for advice concerning the biochemistry of actin.

References and Notes

(1) Pollard, T. D.; Cooper J. A. *Annu. Rev. Biochem.* **1986**, *55*, 978.
(2) Korn, E. D. *Physiol. Rev.* **1982**, *62*, 672.
(3) Aebi, U.; Millonig, R.; Salvo, H.; Engel, A. *Ann. N.Y. Acad. Sci.* **1986**, *483*, 100.
(4) Neuhaus, J.-M.; Wanger, M.; Keiser, T.; Wegner, A. *J. Muscle Res. Cell Motil.* **1983**, *4*, 507.
(5) Yanagida, T.; Nakase, M.; Nishiyama, K.; Oosawa, F. *Nature (London)* **1984**, *307*, 58.
(6) Takebayashi, T.; Morita, Y.; Oosawa, F. *Biochim. Biophys. Acta* **1977**, *492*, 357.
(7) List of the used abbreviations: DTT, dithiothreitol; EGTA, ethylene glycol bis(β-aminoethyl ether)-*N,N,N',N'*-tetraacetic acid; F-buffer, buffer used to polymerize actin (see Materials); FRAP, fluorescence recovery after photobleaching; G-buffer, buffer used to store actin monomers (see Materials); NBD, 7-chloro-4-nitrobenzo-2-oxa-1,3-diazole; QELS, quasielastic light scattering; SDS, sodium dodecyl sulfate; SIT camera, silicon intensified target camera.

(8) Janmey, P. A.; Peetermans, J.; Zaner, K. S.; Stossel, T. P.; Tanaka, T. *J. Biol. Chem.* **1986**, *261*, 8357.
(9) Spudich, J. A.; Watt, S. *J. Biol. Chem.* **1971**, *246*, 4866.
(10) MacLean-Fletcher, S. D.; Pollard, T. D. *Biochem. Biophys. Res. Commun.* **1980**, *96*, 18.
(11) Newman, J.; Estes, J. E.; Selden, L. A.; Gershman, L. C. *Biochemistry* **1985**, *24*, 1538.
(12) Montague, C.; Rhee, K. W.; Carlson, F. D. *J. Muscle. Res. Cell Motil.* **1983**, *4*, 95.
(13) Lanni, F.; Ware, B. R. *Biophys. J.* **1984**, *46*, 97.
(14) Detmers, P.; Weber, A.; Elzinga, M.; Stephens, R. E. *J. Biol. Chem.* **1981**, *256*, 99.
(15) Craig, S. W.; Lancashire, C. L.; Cooper, J. A. *Methods Enzymol.* **1982**, *85*, 316.
(16) Berne, B. J.; Pecora, R. *Dynamic Light Scattering*; Wiley: New York, 1976.
(17) Carlson, F. D.; Fraser, A. B. *J. Mol. Biol.* **1974**, *89*, 273.
(18) Provencher, S. W. *Biophys. J.* **1976**, *16*, 27.
(19) Provencher, S. W. *J. Chem. Phys.* **1976**, *64*, 2772.
(20) Provencher, S. W.; Vogel, R. H. *Math. Biosci.* **1980**, *50*, 251.
(21) Provencher, S. W. *Macromol. Chem.* **1979**, *180*, 201.
(22) Provencher, S. W. *Comput. Phys. Commun.* **1982**, *27*, 213.
(23) Provencher, S. W. *Comput. Phys. Commun.* **1982**, *27*, 229.
(24) Akcasu, A. Z.; Benmouna, M.; Han, C. C. *Polymer* **1980**, *21*, 866.
(25) Gaub, H. E.; Sackmann, E.; Büschl, R.; Ringsdorf, H. *Biophys. J.* **1984**, *45*, 725.
(26) Axelrod, D.; Koppel, D. E.; Schlessinger, J.; Elson, E.; Webb, W. W. *Biophys. J.* **1976**, *16*, 1055.
(27) Engelhardt, H.; Sackmann, E. *Biophys. J.* **1988**, *54*, 495.
(28) Frieden, C. *Proc. Natl. Acad. Sci. U.S.A.* **1983**, *80*, 6513.
(29) Doi, M.; Edwards, S. F. *The Theory of Polymer Dynamics*; Oxford University Press: Oxford, 1986.
(30) Dubois-Violette, E.; de Gennes, P.-G. *Physics* **1967**, *3*, 181.
(31) de Gennes, P.-G. *Physics* **1967**, *3*, 37.
(32) Adam, M.; Delsanti, M. *Macromolecules* **1977**, *10*, 1229.
(33) Nemoto, N.; Makita, Y.; Tsunashima, Y.; Kurata, M. *Macromolecules* **1984**, *17*, 425.
(34) Delsanti, M. Ph.D. Thesis, Orsay, 1978. The references are also given in Chapter 6 of: de Gennes, P.-G. *Scaling Concepts in Polymer Physics*; Cornell University Press: Ithaca, London, 1979.
(35) Rouse, P. E. *J. Chem. Phys.* **1953**, *21*, 1272.
(36) Zimm, B. H. *J. Chem. Phys.* **1956**, *24*, 269.
(37) Benmouna, M.; Akcasu, A. Z. *Macromolecules* **1978**, *11*, 1187.
(38) de Gennes, P.-G. *Macromolecules* **1976**, *9*, 594.
(39) de Gennes, P.-G.; Pincus, P.; Velasco, R. M. *J. Phys. (Les Ulis)* **1976**, *37*, 1461.
(40) de Gennes, P.-G.; Pincus, P.; Velasco, R. M., personal communication, quoted in ref 43.
(41) Gorti, S.; Ware, B. R. *J. Chem. Phys.* **1985**, *83*, 6449.
(42) Turner, D. N.; Hallett, F. R. *Biochim. Biophys. Acta* **1976**, *451*, 305.
(43) Langevin, D.; Rondelez, F. *Polymer* **1978**, *19*, 875, further references therein.
(44) Phillies, G. D. J.; Ullmann, G. S.; Ullmann, K. *J. Chem. Phys.* **1985**, *82*, 5242, further references therein.
(45) Brown, W.; Rymden, R. *Macromolecules* **1986**, *19*, 2942.
(46) Ogston, A. G.; Preston, B. N.; Wells, J. D. *Proc. R. Soc. London, Ser. A* **1973**, *333*, 297.
(47) Altenberger, A. R.; Tirrell, M.; Dahler, J. S. *J. Chem. Phys.* **1986**, *84*, 5122.
(48) Cukier, R. I. *Macromolecules* **1984**, *17*, 252.
(49) Frieden, C. *Annu. Rev. Biophys. Biophys. Chem.* **1985**, *14*, 189.
(50) Sommerfeld, A. *Vorlesungen über Theoretische Physik*; Geest & Portig: Leipzig, 1947.
(51) de Gennes, P.-G. *J. Chem. Phys.* **1971**, *55*, 572.
(52) Tait, J. F.; Frieden, C. *Biochemistry* **1982**, *21*, 6046.
(53) Tait, J. F.; Frieden, C. *Arch. Biochem. Biophys.* **1982**, *216*, 133.
(54) Stossel, T. P.; Chaponnier, C.; Ezzel, R. M.; Hartwig, J. H.; Janmey, P. A.; Kwiatkowski, D. J.; Lind, S. E.; Smith, D. B.; Southwick, F. S.; Yin, H. L.; Zaner, K. S. *Ann. Rev. Cell Biol.* **1985**, *1*, 353.
(55) Kasai, M.; Kawashima, H.; Oosawa, F. *J. Polym. Sci.* **1960**, *44*, 51.
(56) Jen, C. J.; McIntire, L. V.; Bryan, J. *Arch. Biochem. Biophys.* **1982**, *216*, 126.
(57) Sato, M.; Leimbach, G.; Schwarz, W. H.; Pollard, T. D. *J. Biol. Chem.* **1985**, *260*, 8585.
(58) Cortese, J. D.; Frieden, C. *J. Cell Biol.* **1988**, *107*, 1477.
(59) Schmidt, C. F. Ph.D. Thesis, Technical University Munich, 1988.
(60) Fujime, S.; Ishiwata, S.; Maeda, T. *Biophys. Chem.* **1984**, *20*, 1, further references therein.
(61) Nagashima, H.; Asakura, S. *J. Mol. Biol.* **1980**, *136*, 169.
(62) Soda, K. *J. Phys. Soc. Jpn.* **1973**, *35*, 866.
(63) Grimm, H.; Stiller, H.; Majkrzak, C. F.; Rupprecht, A.; Dahlborg, U. *Phys. Rev. Lett.* **1987**, *59*, 1780.
(64) Allegra, G.; Higgins, J. S.; Ganazzoli, F.; Lucchelli, E.; Brückner, S. *Macromolecules* **1984**, *17*, 1253.

Computer Simulation of Copolymer–Copolymer and Copolymer–Homopolymer Mixtures with a Single Interaction Energy

P. Cifra,† F. E. Karasz,* and W. J. MacKnight

Department of Polymer Science and Engineering, University of Massachusetts, Amherst, Massachusetts 01003. *Received September 27, 1988; Revised Manuscript Received February 10, 1989*

ABSTRACT: Interactions in copolymer–homopolymer (A_xB_{1-x}/B) and copolymer–copolymer (A_xB_{1-x}/A_yB_{1-y}) mixtures containing equal amounts of the two respective components were studied as a function of the copolymer compositions x and $|x - y|$, respectively, and of segmental interaction energies using computer simulations of chains on a planar square lattice. The effective interaction parameter χ_{blend} for regimes corresponding to miscibility was less strongly dependent on x (or $|x - y|$) than predicted by the mean-field square power rule, and the number of heterocontacts varied widely from that calculated by random mixing. In the immiscibility regime, the effective χ_{blend} becomes asymptotic as a result of phase separation.

Introduction

Numerical simulations of binary mixtures of homopolymers in either two[1,2] or three[3] dimensions have yielded considerable microscopic information on equilibrium lattice conformations and have permitted examination of the deviations from the mean-field treatment usually applied to such polymer blends. Such computer simulations can readily be performed for a range of interaction energies and have demonstrated effects of mixing, segregation, hole formation, etc., as a function of this parameter.[1-3]

Mixtures of random or near-random copolymers which have received substantial experimental investigation,[4-8] offer an opportunity of examining the effect of additional degrees of freedom in composition and in microsctructure

†Permanent address: Polymer Institute, Slovak Academy of Sciences, 842 36 Bratislava, Czechoslovakia.

0024-9297/89/2222-3649$01.50/0